ARL-TR-9874 ● FEB 2024

Parallel Network Modeling of the Tensile Response of Dyneema SK76 Single Fiber

by Tusit Weerasooriya and Brett Sanborn

NOTICES

Disclaimers

The findings in this report are not to be construed as an official Department of the Army position unless so designated by other authorized documents.

Citation of manufacturer's or trade names does not constitute an official endorsement or approval of the use thereof.

Destroy this report when it is no longer needed. Do not return it to the originator.

ARL-TR-9874 ● FEB 2024

Parallel Network Modeling of the Tensile Response of Dyneema SK76 Single Fiber

Tusit Weerasooriya
DEVCOM Army Research Laboratory

Brett Sanborn
Sandia National Laboratory

REPORT DOCUMENTATION PAGE

1. REPORT DATE	2. REPORT TYPE	3. DATES COVERED	
		START DATE	END DATE
February 2024	Technical Report	1/1/2013	12/31/2014

4. TITLE AND SUBTITLE
Parallel Network Modeling of the Tensile Response of Dyneema SK76 Single Fiber

5a. CONTRACT NUMBER	5b. GRANT NUMBER	5c. PROGRAM ELEMENT NUMBER
5d. PROJECT NUMBER	**5e. TASK NUMBER**	**5f. WORK UNIT NUMBER**

6. AUTHOR(S)
Tusit Weerasooriya and Brett Sanborn

7. PERFORMING ORGANIZATION NAME(S) AND ADDRESS(ES)	8. PERFORMING ORGANIZATION REPORT NUMBER
DEVCOM Army Research Laboratory ATTN: FCDD-RLA-TB Aberdeen Proving Ground, MD 21005	ARL-TR-9874

9. SPONSORING/MONITORING AGENCY NAME(S) AND ADDRESS(ES)	10. SPONSOR/MONITOR'S ACRONYM(S)	11. SPONSOR/MONITOR'S REPORT NUMBER(S)

12. DISTRIBUTION/AVAILABILITY STATEMENT
DISTRIBUTION STATEMENT A. Approved for public release: distribution unlimited.

13. SUPPLEMENTARY NOTES
ORCID ID: Tusit Weerasooriya, 0000-0003-3299-2166

14. ABSTRACT
In this study, experimental uniaxial tensile experiments on Dyneema SK76 single ultra-high molecular weight polyethylene fibers were conducted at strain rates of 0.001/s, 1/s, and 1,000/s. In addition, tensile stress–relaxation and frequency responses from 0 to 170 Hz were also obtained for Dyneema SK76 single fibers. With experimentally measured rate-dependent and stress–relaxation responses, model parameters of two network-based constitutive models were obtained. Although a parallel-networked, second-order time-independent hyperelastic Ogden element with six viscoelastic flow elements was able to capture the rate dependency of Dyneema SK76, the deformation under stress–relaxation behavior was not well represented. The Bergstrom–Boyce (BB) model, which combines time-independent eight-chain Arruda–Boyce elements with BB viscoplastic flow, best described both the rate dependence of the stress–strain responses as well as the nonlinear plastic stress–relaxation deformation behavior at the limiting lower strain rates. Predicted storage and loss moduli frequency responses from both parallel networks were also compared with the measured responses. Although neither model satisfactorily predicted the experimental response, the BB model responses were closer to the experiment, with less error and similar dependency on frequency.

15. SUBJECT TERMS
ultra-high molecular weight polyethylene, Dyneema SK76, constitutive models, parallel network models, Bergstrom–Boyce model, high-rate response, relaxation response, frequency response, Sciences of Extreme Materials, Terminal Effects

16. SECURITY CLASSIFICATION OF:			17. LIMITATION OF ABSTRACT	18. NUMBER OF PAGES
a. REPORT	b. ABSTRACT	C. THIS PAGE		
UNCLASSIFIED	UNCLASSIFIED	UNCLASSIFIED	UU	33

19a. NAME OF RESPONSIBLE PERSON	19b. PHONE NUMBER *(Include area code)*
Tusit Weerasooriya	(410) 652-9450

STANDARD FORM 298 (REV. 5/2020)
Prescribed by ANSI Std. Z39.18

Contents

List of Figures

List of Tables

Acknowledgments

We would like to acknowledge the value of MCalibration optimization software (Veryst Engineering, LLC 2015), which appreciably reduced the time required to obtain the optimized material parameters for the parallel network models that were considered in this research.

1. Introduction

Ultra-high molecular weight polyethylene (UHMWPE) fibers such as Dyneema and Spectra are being used more often in both personnel and vehicle protection applications due to their lower density (0.97 g/cm^3) compared to aramid fibers such as Kevlar and Twaron (1.44 g/cm^3). Additionally, UHMWPE fibers exhibit higher tensile modulus and have good chemical and wear resistance. Numerical simulation of ballistic impact on protective equipment that incorporates these high-performance fibers requires material models of these fibers based on experimental data describing the dependence of deformation and failure on loading rate. Furthermore, such models must capture high-rate material responses relevant to the application scenario.

Existing modeling UHMWPE has been focused on material used in weight-bearing orthopedic components that were primarily based on the J2-plasticity. Bergstrom et al. (2002) showed that the J2-plasticity model did not accurately represent the mechanical behavior of UHMWPE in these applications. Based on more advanced network-based models for glassy polymers, Bergstrom and Bischoff (2010) developed constitutive models based on the physical deformation behavior of the polymer microstructure and found their model to be more accurate than the J2-plasticity-based models. Furthermore, Bergstrom and Bischoff (2010) validated their model based on punch tests of amorphous UHMWPE.

High-performance fibers in protective devices are primarily loaded in a multi-axial stress state within the encased composites, which encompass tension, compression, and shear stresses. They initially deform under such a multi-axial stress state at different strain rates and then fail mainly in either tension or shear dominant mechanisms. In this report, we focus on uniaxial tension, characterize the tensile response as a function of strain rate and gauge lengths, and calibrate model parameters for two numerical models. However, although the models may not represent the actual measured rate-dependent responses completely, researchers tend to choose constitutive models that are currently available in the FE programs such as LS-DYNA (e.g., MAT_076, MAT_S07), because newer models are not well established and cannot be easily incorporated into the widely used simulation software.

In this report, the ability to describe the rate-dependent mechanical deformation response of Dyneema SK76 single fibers is evaluated using two different parallel networking models, consisting of a time-dependent and a time-independent parallel element(s). The first model (HO6LV), chosen for its wider usage is the Maxwell type parallel network model, with a time-independent non-linear response

represented by a second-order Ogden hyperelastic element, combined in parallel with the time-dependent flow represented by six linear viscoelastic flow elements (Ogden 1972). The second model is the advanced (physically based) Bergstrom-Boyce (BB) parallel network model, consisting of time-independent, eight-chain, physically based Arruda-Boyce elements combined with a time-dependent Bergstrom-Boyce nonlinear viscoplastic flow element. BB model has much lesser number of material constants compared to the HO6LV model and is similar to the work published by Bergstrom and Bischoff (2010).

2. Experimental Methods

In this section, details of the material and specimens used for experiments are presented. In addition, the types of experiments and the experimental methods that were used are also discussed.

2.1 Materials

Single fibers were extracted from a spool of 1760 dtex Dyneema SK76 yarns for all experiments. To obtain valid experimental data for numerical models for Dyneema SK76, a direct gripping method was used (Sanborn et al. 2015). This method consists of mounting a single fiber in a cardstock specimen holder. The specimen is then inserted into the grips and the grip covers are tightened to secure the fiber. The cardstock holder is then clipped away leaving only the single fiber spanning the gauge length. This direct gripping method has been demonstrated to squeeze and hold individual fiber specimens with enough force such that the fiber can be loaded to failure within the gauge area away from the grips. This method allows a wide range of diameters to be gripped without apparent slipping. To understand any fiber-gauge length effects, multiple gauge lengths were studied. At quasi-static and intermediate rate, experiments on gauge lengths of 5, 10, and 50 mm were studied whereas at high-rate experiments were conducted on 5-, 7-, and 10-mm specimens.

A 30-cm-long, single fiber was used to make several fiber samples. Rows of aligned specimen holders were fabricated using a laser cutter. The 30-cm-long fibers were glued across these rows, and then the individual specimens were extracted. To avoid confounding factors due to variability in diameter of the single-fiber specimens, the diameter of each specimen was carefully measured using an optical microscope. For each sample, 10–20 measurements were taken at different locations along the length and were averaged to obtain the diameter. A total of 276 samples were measured for this study and the diameter was 18.22 ± 1.15 μm.

2.2 Uniaxial Tension

Sanborn et al. (2015) provided complete details of the method used and the unique gripping methods that were developed for the tensile experiments that were conducted to obtain rate dependency. A summary of these experiments is given here. All tensile experiments were conducted until failure, characterized as catastrophic separation of the fiber in the gauge length into two separate parts. A Bose Electroforce test bench was used to pull single Dyneema SK76 fibers in tension at strain rates of 0.001 s^{-1} and 1 s^{-1}. The strain (ε, Eq. 1) and strain rate ($\dot{\varepsilon}$, Eq. 2) are calculated based on the gauge length (l_s) of the sample:

$$\varepsilon = \frac{d}{l_s}, \tag{1}$$

$$\dot{\varepsilon} = \frac{v}{l_s}, \tag{2}$$

where a is the displacement of actuator and v is the velocity of the experiment. The specimen stress is calculated as follows (Eq. 3):

$$\sigma = \frac{P}{A_0}, \tag{3}$$

where A_o is the initial cross-sectional area based upon the diameter measurement obtained using optical microscopy for each sample. Finally, P is the force measured by the load cell.

To study the high-rate behavior of Dyneema SK76 for numerical modeling purposes, a fiber-split Hopkinson tension bar (SHTB) was used as shown in Fig. 1 to obtain material response at strain rates of approximately 1,000 s^{-1}. The setup shown in Fig. 1 has been used by several authors to study the rate-dependent response of ballistic fibers, including several grades of Kevlar and Dyneema (Cheng et al. 2005; Sanborn et al. 2015).

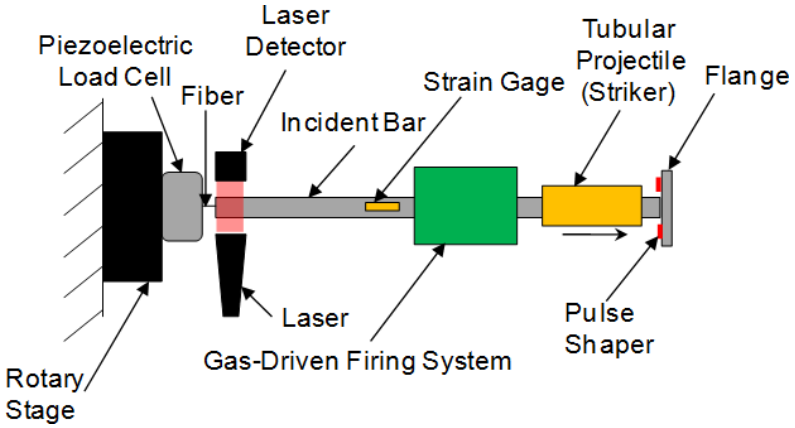

Fig. 1 Schematic of fiber-SHTB

The fiber-SHTB uses a tubular projectile fired using compressed gas from a barrel toward the impact flange. Upon contact with the flange, a tensile pulse is generated in the bar, which propagates down the bar and pulls the specimen in tension. Force is recorded using a fast-acting piezoelectric load cell due to the weak response of the fiber. A thin copper pulse shaper is used to control the rise time of the incident pulse. Equations 1, 2, and 3 are all used to obtain the strain rate, strain, and stress history. The displacement measurement of the bar end is obtained through use of a laser extensometer located at the specimen end of the incident bar. Before experimentation, a voltage-displacement relation is obtained by incrementally uncovering the laser.

2.3 Dynamic Mechanical Analysis Experiments

In addition to studying the uniaxial tensile behavior at quasi-static, intermediate, and high strain rates, dynamic mechanical analysis (DMA) experiments were conducted to characterize the storage and loss moduli of Dyneema SK76. Using the DMA module of the Bose Electroforce, frequency sweep experiments were conducted over a range of 0–170 Hz. Mean strains of 1% or 2% were used with strain amplitude held constant at 0.5%.

2.4 Stress Relaxation

Along with DMA experiments, the stress–relaxation behavior was studied using the Bose Electroforce. Fibers were pulled in tension at either 0.001 s^{-1} or 1 s^{-1} and held for a period of 300 s. At each strain rate, five 10-mm gauge length samples were pulled in tension to study the stress–relaxation behavior of the material.

3. Results and Discussion

3.1 Stress–Strain Response as a Function of Rate

The stress–strain behavior of Dyneema SK76 single fibers for 5-mm gauge length at quasi-static rate is shown in Fig. 2. Most of the experimental results shown in this section are previously reported in detail by Sanborn et al. (2015). These experiments show a high amount of repeatability and agreement with the experimental results of Russell et al. (2013) on SK76. Figure 2 also shows that the behavior of Dyneema SK76 is not linear at quasi-static strain rates like fibers such as Kevlar KM2 (Cheng et al. 2005).

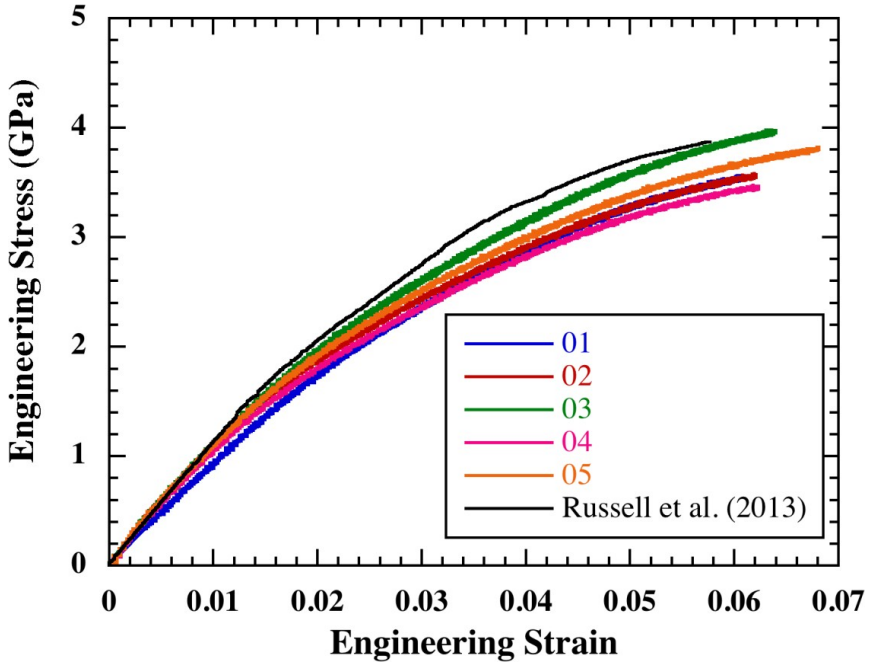

Fig. 2 Typical stress–strain curves of Dyneema SK76 single fibers from quasi-static experiments (5-mm gauge length) including the results of Russell et al. (2013). Gauge length is not given in the Russell et al. (2013).

Figure 3 shows high-rate stress strains for 5-mm gauge length. The shape of the deformation response and the slope of the initial elastic loading regime were approximately similar for the other gauge lengths, contrary to the results for failure strengths, which showed appreciable dependence on gauge length. While these results are highly repeatable as in the quasi-static case, the shape of the stress–strain curve is more linear than the quasi-static case. Including the intermediate strain-rate results that are shown in Fig. 4, the shape of the stress–strain curve becomes increasingly linear with increasing strain rate, which has been reported previously (Cansfield et al. 1983; Schwartz et al. 1986; Russell et al. 2013). Figure 4 also indicates that there was not an appreciable difference in the stress–strain response as a function of the gauge length of the specimens, such that data from either gauge length could be used in model calibration.

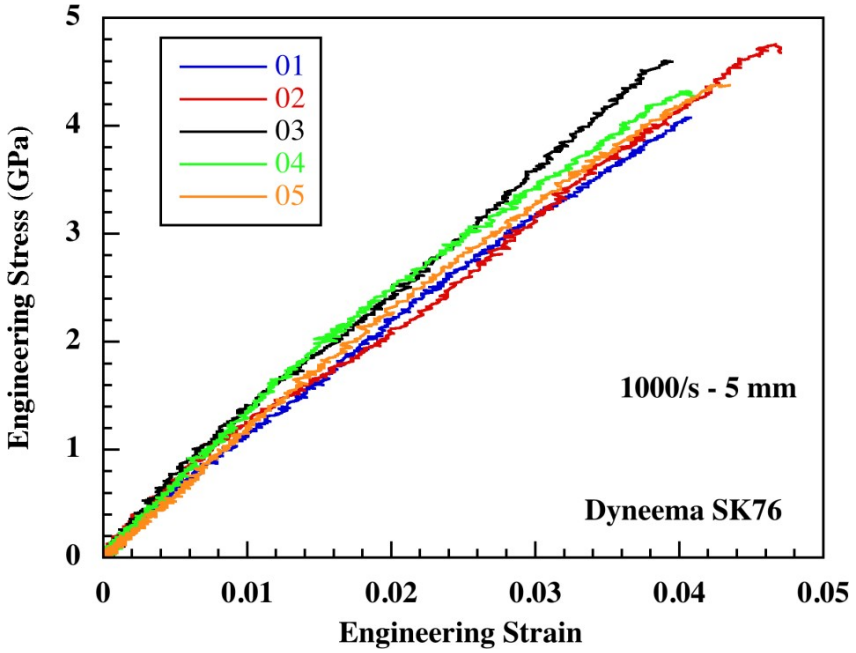

Fig. 3 High-rate stress–strain curves for Dyneema SK76 with 5-mm gauge length

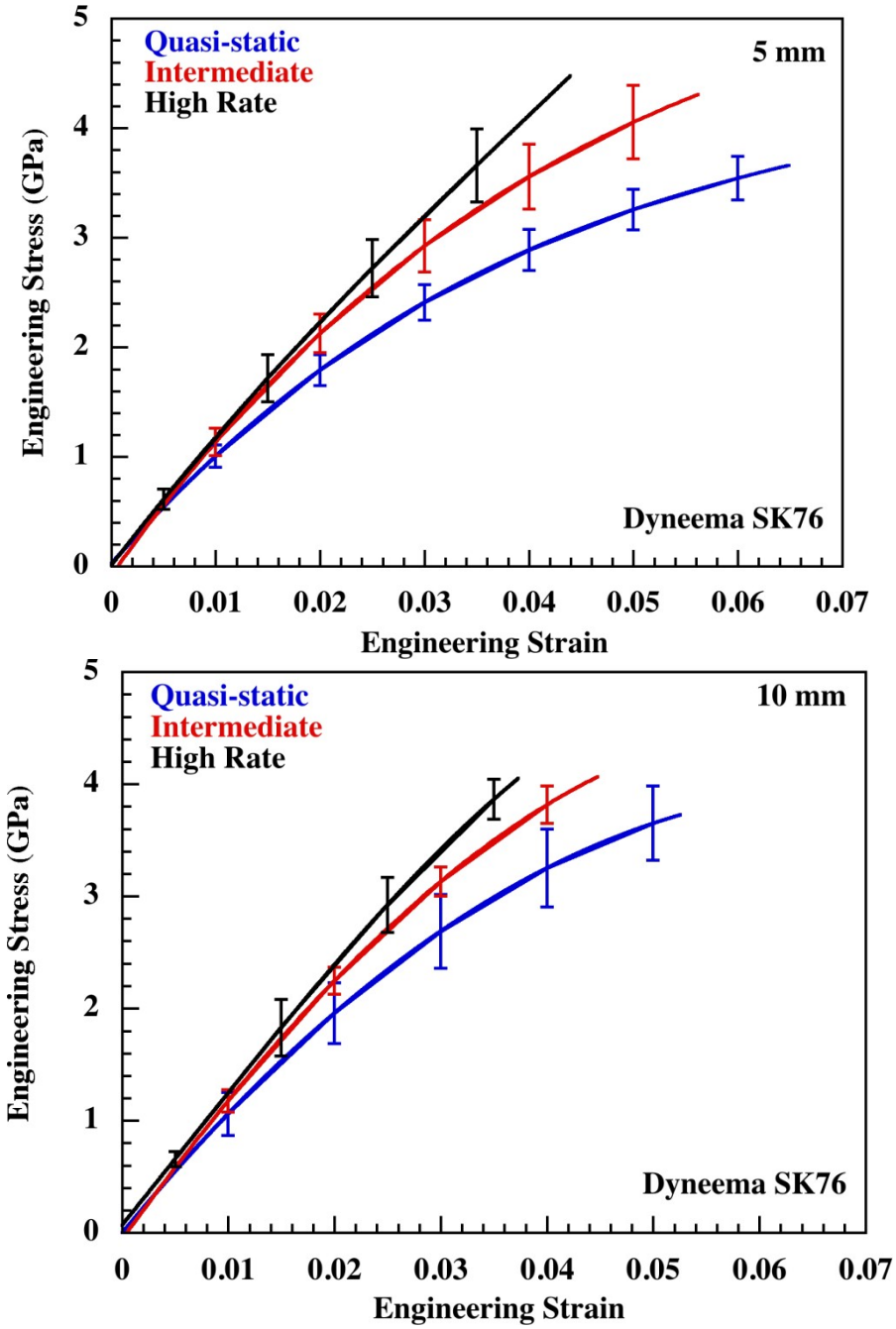

Fig. 4 Stress–strain response of Dyneema SK76 single fibers at multiple strain rates for 5- (top) and 10-mm (bottom) gauge lengths. Note the increase in linearity for the same gauge length with increasing strain rate. The curves in these plots represent the average behavior of 10 experiments with error bars representing ±1 standard deviation.

Figure 5 and Table 1 show the failure strength in uniaxial tension as a function of strain rate. Error bars in Fig. 5 represent ±1 standard of deviation. The results of another study on Dyneema SK76 by Hudspeth et al. (2012) are also plotted in Fig. 5. In general, we noted an increasing relationship between failure strength and strain

rate up to a strain rate of 1 s^{-1}. After a strain rate of 1 s^{-1} is reached, no increase in strength is recorded when the strain rate is further increased to approximately 1,000 s^{-1}. The results in Fig. 5 also indicate the absence of specimen gauge-length effects evidenced by the similarity in strength of the three gauge-length fibers tested at each strain rate.

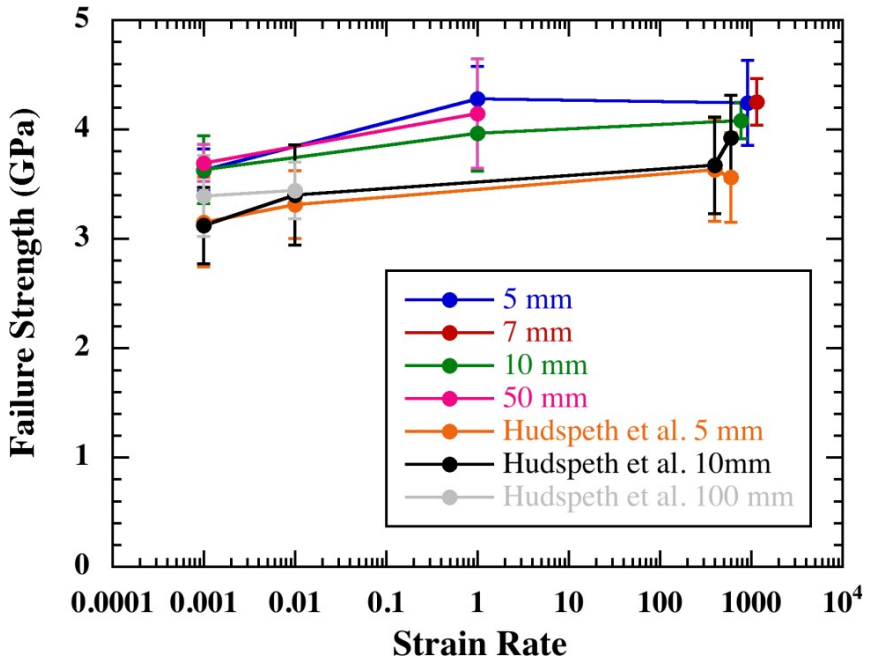

Fig. 5 Strain-rate dependence of the failure strength of Dyneema SK76 single fibers loaded in uniaxial tension with data from Hudspeth et al. (2012)

Table 1 Failure strengths of Dyneema SK76 at different strain rates and gauge lengths

Strain rate (s^{-1})	5-mm strength (GPa)	7-mm strength (GPa)	10-mm strength (GPa)	50-mm strength (GPa)
0.001	3.63 ± 0.19	…	3.64 ± 0.31	3.69 ± 0.17
1	4.28 ± 0.30	…	3.96 ± 0.35	4.14 ± 0.50
775	…	…	4.08 ± 0.17	…
913	4.24 ± 0.39	…	…	…
1,156	…	4.25 ± 0.21	…	…

3.2 Cyclic Response to Small Amplitude Loading: Storage and Loss Moduli

The response of the fibers evaluated under small amplitude vibratory loading conditions over a range of frequencies from 10 to 170 Hz at room temperature are shown in Fig. 6, and a typical frequency sweep response from a single experiment is shown in Table 2. The storage (E') and loss (E'') moduli were calculated from experimental measurements using Fourier transforms of the input and output sinusoidal loading and strain waves for each frequency.

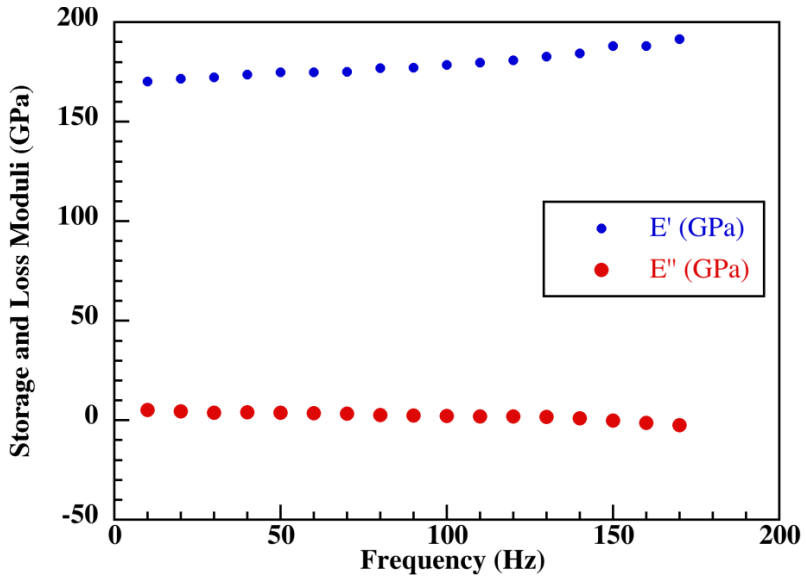

Fig. 6 Storage and loss moduli as a function of frequency for Dyneema SK76

Table 2 Typical frequency sweep response of Dyneema SK76

ε-mean (%)	ε-amp	Frequency (Hz)	E' (MPa) (0.0075 A)	E" (MPa) (0.0075 A)	Tan delta	T (°K)
1.0059	0.50167	10	15881043	448775.2	0.028247	293
1.0137	0.5438	20	16121984	369768.2	0.022917	293
1.002	0.53231	30	16155029	329655.5	0.020379	293
1.0326	0.53231	40	16254676	312016	0.019158	293
1.0003	0.57443	50	16233159	332110.4	0.0204	293
1.0059	0.53231	60	16382129	278418.4	0.016934	293
1.0097	0.55337	70	16443945	251619.9	0.015232	293
1.0212	0.53997	80	16568508	195458.6	0.011733	293
0.99994	0.52082	90	16632351	170837.9	0.010204	293
1.0039	0.52273	100	16749754	162187.9	0.009607	293
1.0061	0.51507	110	16812710	130623.8	0.007698	293
1.0058	0.52465	120	16946080	137140.2	0.008005	293
1.0003	0.52656	130	17104232	119191.8	0.006882	293
1.0003	0.52273	140	17270087	37151.88	0.002122	293
1.0022	0.52082	150	17607285	−24778.6	−0.00139	293
1.0097	0.52273	160	17593897	−174936	−0.00979	293
1.0002	0.53039	170	17798101	−930986	−0.05182	293

3.3 Stress Relaxation

Typical stress–relaxation plots for Dyneema SK76 at two strain rates are shown in Fig. 7. Fibers were loaded to approximately 3% strain and held for a period of 300 s. At both strain rates, the Dyneema SK76 fiber displays viscoelastic behavior as seen by the relaxation of stress when the sample was held at constant strain. After releasing the applied strain, the fibers did not recover to the original gauge length.

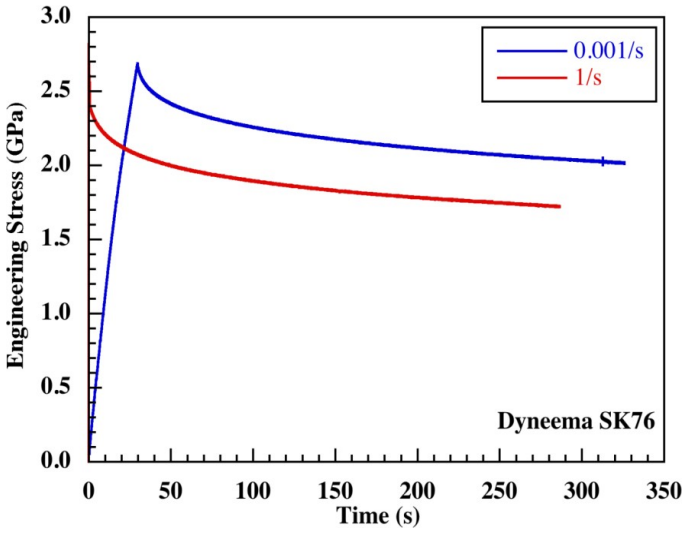

Fig. 7 Stress–relaxation behavior of Dyneema SK76 single fibers at two strain rates

4. Parallel Network Constitutive Models

Several constitutive models were evaluated using MCalibration (Veryst Engineering, LLC 2015) error optimizer software to determine their ability to represent the experimentally obtained stress–strain response at multiple loading rates.

4.1 HO6LV Model: Parallel Network Consisting of a Time-Independent Second-Order Hyperelastic Ogden Element in Parallel with Six Time-Dependent Linear Viscoelastic Element

A parallel network model consisting of a time-independent hyperelastic second-order Ogden element in parallel with time-dependent linear viscoelastic elements was evaluated. In this study, the number of viscoelastic elements was restricted to six, and the model was therefore identified as HO6LV. Figure 8 presents a schematic of this model.

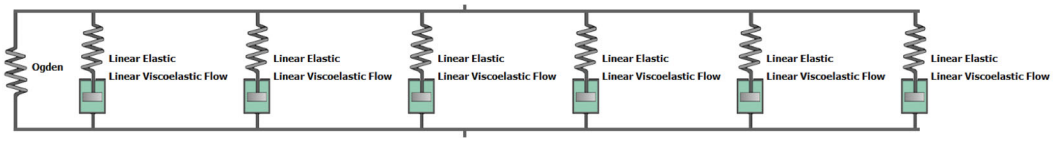

Fig. 8 Schematic representation HO6LV model

In the second-order, hyperelastic Ogden element, the principal stress (σ) is as follows (Eq. 4):

$$\sigma = \sum_{i=1}^{2} \mu_{oi}(\lambda^{\alpha_{oi}} - \lambda^{\frac{\alpha_{oi}}{2}})/\lambda, \tag{4}$$

where λ is the stretch ratio based on the change in length, and μ and α are material constants.

The viscoelastic part of the model is represented by the Prony series (Eq. 5),

$$E(t) = \sum_{i=1}^{6} E_i \, e^{\left(-\frac{t}{\hat{\tau}_i}\right)}, \tag{5}$$

where E is the stiffness and $\hat{\tau}$ is the relaxation time of each linear viscoelastic element.

The model prediction using the HO6LV is shown in Fig. 9, with model constants given in Table 3. This HO6LV model does a fair job in capturing the rate-dependent behavior of Dyneema SK76. However, Fig. 9 shows that even though the model predicts the experimentally observed linear behavior at high rate, the ability of the model to predict the experimental behavior decreases as the strain rate decreases. In addition, the HO6LV model does not reproduce the correct stress–relaxation behavior of the fiber at the limiting low strain rate as shown in Fig. 10, despite using six linear viscoelastic elements.

Table 3 Model constants for the HO6LV model

Description	Symbol	Value
OgdenModulus1 (GPa)	μ_{o1}	27.3824
OgdenExponent1 (GPa)	α_{o1}	−14.2697
OgdenModulus2 (GPa)	μ_{o2}	0.0160
OgdenExponent2 (GPa)	α_{o2}	0.5308
Modulus1 (GPa)	E_1	0.5308
Time constant1 (s)	$\hat{\tau}_1$	100.0000
Modulus2 (GPa)	E_2	1.6263
Time constant2 (s)	$\hat{\tau}_2$	10.0000
Modulus3 (GPa)	E_3	23.9112
Time constant3 (s)	$\hat{\tau}_3$	1.0000
Modulus4 (GPa)	E_4	10.2784
Time constant4 (s)	$\hat{\tau}_4$	0.1000
Modulus5 (GPa)	E_5	2.0554
Time constant5 (s)	$\hat{\tau}_5$	0.0100
Modulus6 (GPa)	E_6	0.3996
Time constant6 (s)	$\hat{\tau}_6$	0.0010
R^2 for quality of the fit	…	0.7330

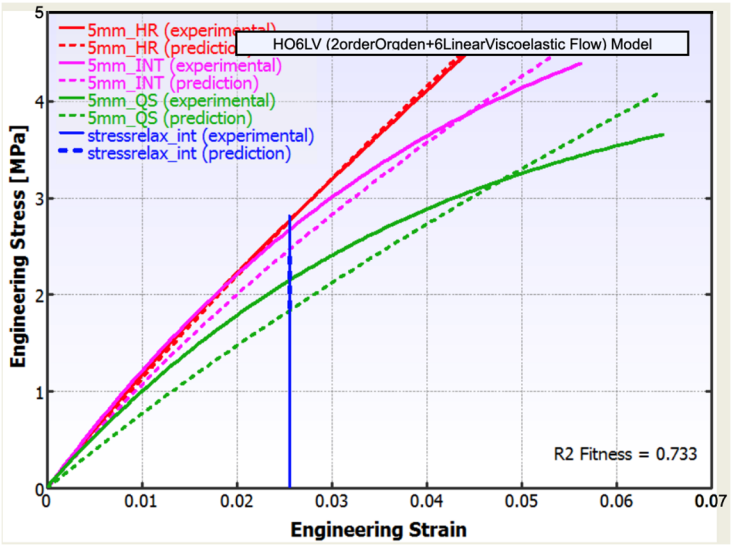

Fig. 9 Stress–strain response of Dyneema SK76 single fiber comparing experiments from present study (solid lines) to a second-order HO6LV (dashed lines)

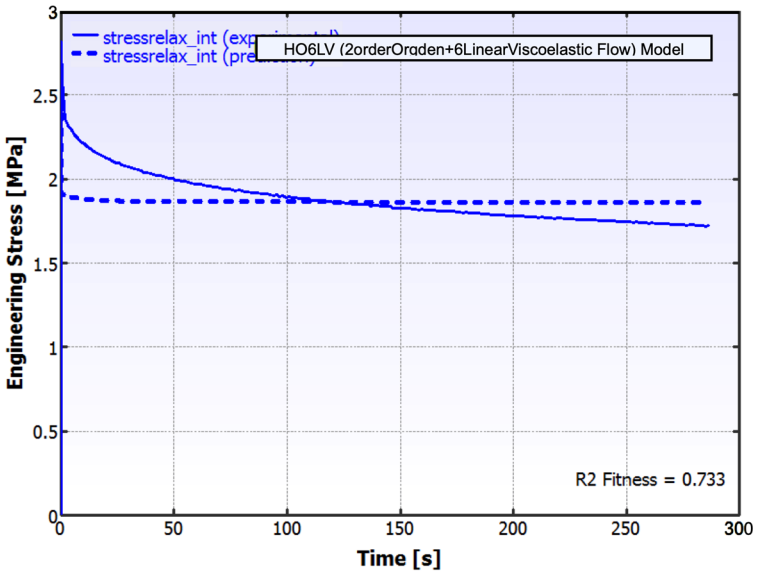

Fig. 10 HO6LV model prediction (dashed line) of the experimentally measured stress–relaxation behavior (solid line) of Dyneema SK76 loaded in uniaxial tension at intermediate rate

4.2 BB Model: Parallel Network of Time-Independent Eight-Chain Arruda–Boyce Elements with a Time-Dependent Bergstrom-Boyce Flow Element

The BB model consisted of time-independent eight-chain Arruda–Boyce elements combined with a time-dependent Bergstrom-Boyce flow element. This model has been shown to predict the time-dependent behavior of polymeric materials (Bergstrom and Boyce 1998). The BB model is based on a deformation gradient acting on two parallel networks, A and B (Fig. 11), such that $\boldsymbol{F} = \boldsymbol{F}_A = \boldsymbol{F}_B$. Here, bold symbol represents the second-order tensor or matrix. Network A represents the equilibrium response of the material using the eight-chain Arruda–Boyce model with one hyperelastic element, whereas network B represents the time-dependent response in which a hyperelastic element is in series with a time-dependent element. The deformation gradient of network B is divided into elastic and viscoplastic components $\boldsymbol{F}_B = \boldsymbol{F}_B^e \cdot \boldsymbol{F}_B^{vp}$. The detailed derivation of the 3D theory and uniaxial simplification can be found in Arruda and Boyce (1993) and Bergstrom and Boyce (1998, 1999, 2000).

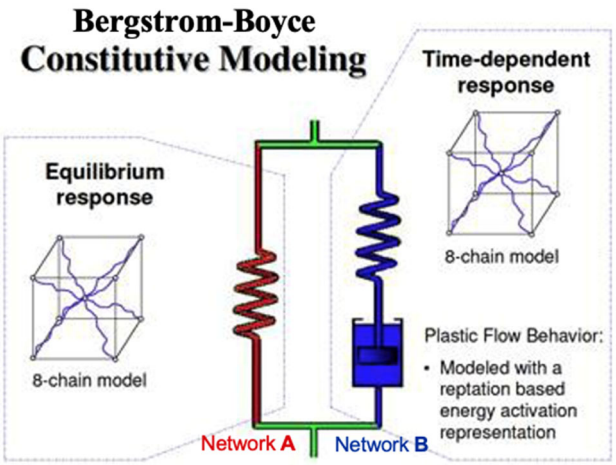

Fig. 11 BB model for polymeric materials (Bergstrom and Boyce 1998)

The Cauchy stress for this formulation is given by $\sigma = \sigma_A + \sigma_B$, where A and B represent each network in the model. Stress components σ_A and σ_B are given as follows (Eqs. 6 and 7):

$$\sigma_A = \frac{\mu_A}{\lambda} \cdot \frac{\mathcal{L}^{-1}\left(\bar{\lambda}/\lambda_A^L\right)}{\mathcal{L}^{-1}\left(1/\lambda_A^L\right)}\left[\boldsymbol{F}^2 - \frac{1}{\boldsymbol{F}}\right], \tag{6}$$

and

$$\sigma_B = \frac{s\cdot\mu_A}{\lambda_B^e} \cdot \frac{\mathcal{L}^{-1}\left(\bar{\lambda}_B^e/\lambda_B^L\right)}{\mathcal{L}^{-1}\left(1/\lambda_B^L\right)}\left[(\boldsymbol{F}_B^e)^2 - \frac{1}{\boldsymbol{F}_B^e}\right], \tag{7}$$

where s is a dimensionless material parameter relating the shear modulus of network B to network A, and μ_A and $\mu_B = s\mu_A$ are the shear moduli, and λ_A^L and λ_B^L are the limiting chain stretch for networks A and B, respectively. $\mathcal{L}^{-1}(x)$ is the inverse of the Langevin function, which is given by $\mathcal{L}(x) = \coth(x) - 1/x$ and is approximated as follows (Eq. 8):

$$\mathcal{L}^{-1}(x) \approx \begin{cases} 1.31446\ \tan(1.58986x) + 0.91209x, & if\ |x| < 0.84136 \\ 1/(\text{sign}(x) - x), & if\ 0.84136 \le |x| < 1 \end{cases} \tag{8}$$

The stretch terms of each network are as follows (Eqs. 9 and 10):

$$\bar{\lambda} = \sqrt{\frac{1}{3}\left[(\boldsymbol{F})^2 + \frac{2}{\boldsymbol{F}}\right]}, \tag{9}$$

and

$$\bar{\lambda}_B^e = \sqrt{\frac{1}{3}\left[(\boldsymbol{F}_B^e)^2 + \frac{2}{\boldsymbol{F}_B^e}\right]}. \tag{10}$$

For network B, the rate equation for viscous flow is as follows (Eq. 11):

$$\dot{\gamma}_B^{vp} = \dot{\gamma}_0\left(\bar{\lambda}_B^{vp} - 1 + \xi\right)^C \left[R\left(\frac{2|\sigma_B|}{3\tau_{base}}\right)\right]^m, \tag{11}$$

where $\dot{\gamma}_0 = 1/s$ is a constant for dimensional consistency. The ramp function R is (Eq. 12)

$$R(x) = (x + |x|)/2, \tag{12}$$

and the stretch term $\bar{\lambda}_B^{vp}$ is as follows (Eq. 13):

$$\bar{\lambda}_B^{vp} = \sqrt{\frac{1}{3}\left[\left(\boldsymbol{F}_B^{vp}\right)^2 + \frac{2}{\boldsymbol{F}_B^{vp}}\right]}, \tag{13}$$

where C, ξ, τ_{base}, and m are material constants.

With the viscous flow given in Eq. (11), the viscoplastic deformation gradient ($\boldsymbol{F}_B$) of network B is given by the following (Eq. 14):

$$\dot{\boldsymbol{F}}_B^{vp} = \dot{\gamma}_B^{vp} \cdot sign[\sigma_B] \cdot \boldsymbol{F}_B^{vp}. \tag{14}$$

The prediction of the stress–strain behavior using BB model is shown in Fig. 12, and a table of the model constants can be found in Table 4. Like the Ogden model, the BB model captures the strain-rate behavior of the fiber over the wide range of strain rates up to 1000 s^{-1}. Unlike the HO6LV model, the BB model captures the rate-dependent, stress–strain response of the Dyneema SK76 fiber fairly well across loading rates, especially at high strain rate where the response is almost linear. The BB model also is accurately predicting the stress–relaxation behavior of Dyneema SK76 fiber (Fig. 13).

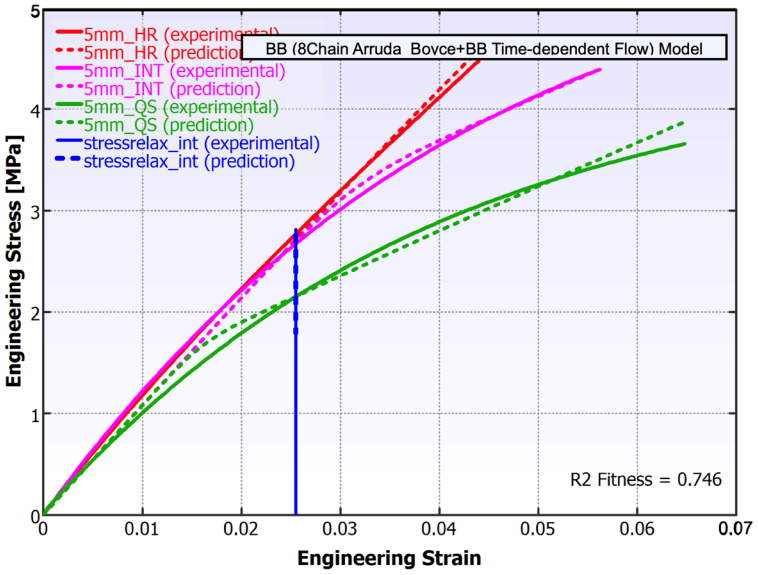

Fig. 12 BB model prediction (dashed lines) for Dyneema SK76 single fibers at multiple strain rates compared to the experiment (solid lines)

Table 4 Model constants for BB model

Description	Symbol	Value
Modulus of network A (GPa)	μ_A	16.2019
Locking stretch for network A	λ_A^L	4.8724
Modulus of network B (GPa)	$\mu_B = s\mu_A$	20.6210
Locking stretch for network B	λ_B^L	9.8282
Strain adjustment factor	ξ	0.0100
Strain exponent	C	−1.9613
Flow resistance (GPa)	τ_{base}	3.7401
Stress exponent	m	10.2134
R^2 for quality of the fit	...	0.7460

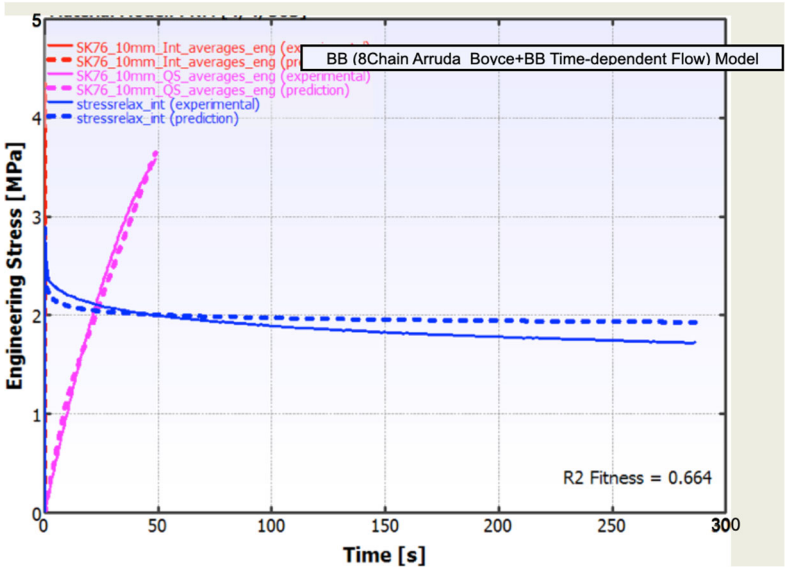

Fig. 13 BB model prediction (dashed line) for stress relaxation compared with the experiment (solid line) for Dyneema SK76 single fibers loaded in uniaxial tension at intermediate rate

4.3 Comparison of Experimental and Predicted Storage and Loss Moduli as a Function Frequency

Both HO6LV and BB models with the optimized model parameters were used to predict DMA storage and loss moduli response from DMA experiments as function of frequency. Figure 14 shows the comparison of predicted and experimental frequency responses. Figure 15 shows the comparison of storage and loss moduli responses as a function for prediction from the BB model and the experiment. The mCalibration software was unable to obtain model constants for both models, when the frequency response data were also used in the optimization process. BB model

prediction followed the trend of the experiments with lower error compared to HO6LV model prediction.

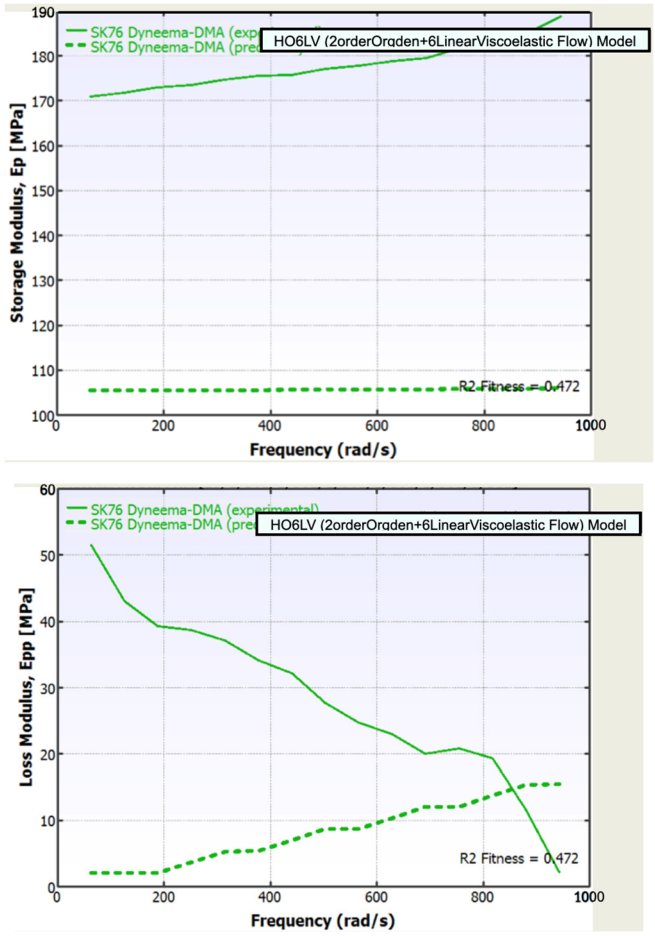

Fig. 14 HO6LV model prediction (dashed lines) of storage and loss moduli response for Dyneema SK76 as a function of frequency compared to experimental response (solid lines)

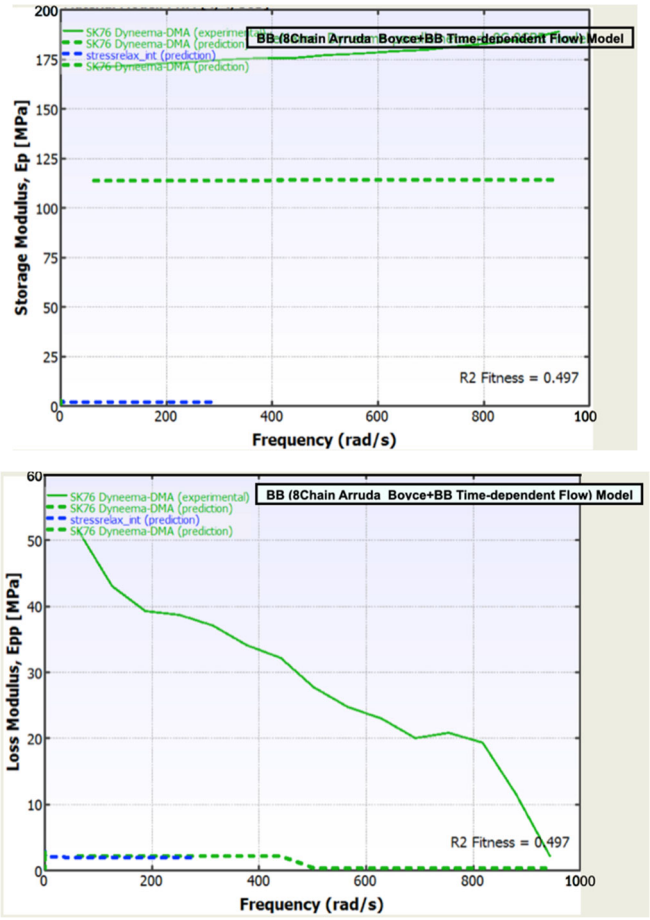

Fig. 15 BB model prediction (dashed lines) of storage and loss moduli response for Dyneema SK76 as a function of frequency compared to experimental response (solid lines)

5. Conclusion

Uniaxial tensile experiments on Dyneema SK76 single fibers were conducted at strain rates of 0.001/, 1/s, and 1,000/s. In addition, tensile stress–relaxation experiments were also conducted. Using the experimentally measured mechanical responses, model parameters were obtained for two parallel network constitutive models by minimizing the error between experimental and model responses using the mCalibration software from Veryst Engineering, LLC (2015). Although the HO6LV model captured the rate dependence of Dyneema SK76, the creep-like plastic deformation behavior at low rates is not well represented by this model. Our results show that the BB model best describes both the rate dependency of the stress–strain curves as well as the nonlinear creep-like plastic deformation behavior for the limiting lower strain rate. In addition, the HO6LV model could not represent either the amplitudes or the trends of frequency response of the moduli, whereas the BB model was able to capture the trends with lower errors in amplitudes of the frequency response, compared to that from HO6LV. The simpler and well-known

Maxwell HO6LV model can be easily implemented in commercial FE software such as LS-DYNA, whereas implementation of the BB model is comparatively more challenging. The present findings provide an understanding of the limitations of the well-known Maxwell viscoelastic models compared to more complex, physically based BB model.

6. References

Arruda EM, Boyce MC. A three-dimensional constitutive model for the large stretch behavior of rubber elastic materials. J Mech Phys Solids. 1993;41(2):389–412. https://doi.org/10.1016/0022-5096(93)90013-6.

Bergstrom JS, Boyce MC. Constitutive modeling of the large strain time-dependent behavior of elastomers. J Mech Phys Solids. 1998;46:931–954. https://doi.org/10.1016/S0022-5096(97)00075-6.

Bergstrom JS, Boyce MC. Mechanical behavior of particle filled elastomers. Rubber Chem Technol. 1999;72:633–656. https://doi.org/10.5254/1.3538823.

Bergstrom JS, Boyce MC Large strain time-dependent behavior of filled elastomers. Mech Mater. 2000;32:620–644. https://doi.org/10.1016/S0167-6636(00)00028-4.

Bergstrom JS, Bischoff JE. An advanced thermomechanical constitutive model for UHMWPE. Int J Struct Changes Solids. 2010; 2(1):31–39. https://ijscs-ojs-tamu.tdl.org/ijscs/index.php/ijscs/article/view/2350.

Bergstrom J, Kurtz S, Rimnac C, Edidin A. Constitutive modeling of ultra-high molecular weight polyethylene under large-deformation and cyclic loading conditions. Biomaterials. 2002;23:2329–2343. https://doi.org/10.1016/S0142-9612(01)00367-2.

Cansfield D, Ward I, Woods D, Buckley A, Pierce J, Wesley J. Tensile strength of ultra high modulus linear polyethylene filaments. Polym Commun. 1983;24:130e1.

Cheng M, Chen W, Weerasooriya T. Mechanical properties of Kevlar KM2 single fiber. J Eng Mater Technol. 2005;127:197–203. https://doi.org/10.1016/j.ijsolstr.2004.05.016.

Hudspeth M, Nie X, Chen W. Dynamic failure of Dyneema SK76 single fibers under biaxial shear/tension. Polymer. 2012;53:5568–5574. https://doi.org/10.1016/j.polymer.2012.09.020.

Ogden RW. Large deformation isotropic elasticity - on the correlation of theory and experiment for incompressible rubberlike solids. Proceedings of the Royal Society of London. Series A, Mathematical and Physical Sciences; 1972;326(1567):565–584. https://doi.org/10.1098/rspa.1972.0026.

Veryst Engineering, LLC. PolyUMod™ and MCalibration User Manuals. 2015 [accessed 2024 Jan 17].

https://polymerfem.com/polymer_files/MCalibration_Introduction.pdf;
https://www.veryst.com/services/material-modeling/material-model-calibration.

Russell BP, Karthikeyan K, Deshpande VS, Fleck NA. The high strain rate response of ultra high molecular weight polyethylene: from fibre to laminate. Int J Impact Eng. 2013;60:1–9. https://doi.org/10.1016/j.ijimpeng.2013.03.010

Sanborn B, DiLeonardi AM, Weerasooriya T. Tensile properties of Dyneema SK76 single fibers at multiple loading rates using a direct gripping method. J Dyn Behav Mater. 2015;1:4–14. https://doi.org/10.1007/s40870-014-0001-3. https://apps.dtic.mil/sti/pdfs/ADA606636.pdf.

Schwartz P, Netravali A, Sembach S. Effects of strain rate and gauge length on the failure of ultrahigh strength polyethylene. Textile Res J. 1986;56(8):502–508. https://doi.org/10.1177/004051758605600807.

List of Symbols, Abbreviations, and Acronyms

3D	3-dimensional
DMA	dynamic mechanical analysis
EMS	elemental macro-scale
FE	finite element
HO6LV	hyperelastic Ogden model with six elements
SHTB	split Hopkinson tension bar
SMS	sub-mesoscale
UHMWPE	ultra-high molecular weight polyethylene

1 (PDF) DEFENSE TECHNICAL INFORMATION CTR
DTIC OCA

1 (PDF) DEVCOM ARL
FCDD RLD DCI
TECH LIB

12 (PDF) DEVCOM SC
MG CARBONI
D COLANTO
R DILLALLA
B FASEL
J FONTECCHIO
B KIMBALL
J KIREJCZYK
J PARKER
M MAFEO
M MARKEY
D OTTERSON
D PHELPS

2 (PDF) PEO SOLDIER
J HOPPING
J MULLENIX

1 (PDF) PEO IEWS
A FOURNIER

1 (PDF) MTRL SCIENCES DIV
LAWRENCE BERKELY NATL LAB
R RITCHIE

5 (PDF) SOUTHWEST RSRCH INST
C ANDERSON JR
S CHOCRON
D NICOLELLA
T HOLMQUIST
G JOHNSON

2 (PDF) NIST
A FORSTER
M VANLANDINGHAM

1 (PDF) INST FOR DEFNS ANLYS
Y MACHERET

3 (PDF) MRMC DOD BLAST INJURY RSRCH PROGRAM COOR OFC
R GUPTA
T PIEHLER
R SHOGE

2 (PDF) MRMC JTAPIC PRGM OFC
W LEI
J USCILOWICZ

4 (PDF) US ARMY AEROMEDICAL RSRCH LAB
F BROZOSKI
V CHANCEY
B MCENTYRE
D WISE

1 (PDF) DEVCOM GVSC
R SCHERER

1 (PDF) DEVCOM C5ISR
AMSRD PE
D RUSIN

2 (PDF) DEVCOM CBC
M HORSMON
N VINCELLI

1 (PDF) OSD DOT&E
J IVANCIK

5 (PDF) US NAVAL RSRCH LAB
A BAGCHI
A ILIOPOULOS
J MICHOPOULOS
K TEFERRA
X TAN

4 (PDF) DAC
FCDD DAG S
K LOFTIS
FCDD DAS LBE
J GURGANUS
S SNEAD
FCDD DAS LBW
G DIETRICH

105 (PDF) DEVCOM ARL
FCDD RLD
J RIDDICK
FCDD RLA A
S KARNA
J NEWILL
A RAWLETT
S SCHOENFELD
J ZABINSKI
N ZANDER
FCDD RLA B
R BECKER
J CAMPBELL
P GILLICH
C HOPPEL
B SCHUSTER
A TONGE
M TSCHOPP
L VARGAS-GONZALEZ
FCDD RLA H
T THOMAS
FCDD RLA HC
A DAGRO
A EIDSMORE
FCDD RLA M
R BRENNEN
E CHIN
FCDD RLA MA
K BERNETICH
T BOGETTI
S BOYD
J CAIN
M NEBLETT
T PLAISTED
F RACINE
E SANDOZ-ROSADO
J SANDS
J STANISZEWSKI
E WETZEL
M YEAGER
CF YEN
FCDD RLA MB
G GAZONAS
B LOVE
P MOY
D O'BRIEN
J SIETINS
J SUN
T WALTER
FCDD RLA MC
R JENSEN
FCDD RLA MD
A BUJANDA
B CHEESEMAN
K CHO
J LA SCALA
S WALSH
FCDD RLA ME
J LASALVIA
P PATEL
S SILTON
J SWAB
FCDD RLA MF
K DARLING
S GRENDAHL
C HAINES
H MURDOCH
FCDD RLA MG
J ANDZELM
J LENHART
R MROZEK
FCDD RLA T
R FRANCART
FCDD RLA TA
S BILYK
FCDD RLA TB
S ALEXANDER
T BAUMER
A BROWN
B FAGAN
A GOERTZ
A GUNNARSSON
C HAMPTON
M KLEINBERGER
E MATHEIS
J MCDONALD
P MCKEE
K RAFAELS
S SATAPATHY
M TEGTMEYER
T WEERASOORIYA
S WOZNIAK
T ZHANG
FCDD RLA TC
J CAZAMIAS
D CASEM
J CLAYTON
C MEREDITH
L SHANNAHAN
J LLOYD
FCDD RLA TD
R DONEY
R GUPTA
B KRZEWINSKI
K MASSER
F MURPHY
C RANDOW
B SCOTT
M ZELLNER
FCDD RLA TE
M LOVE
P SWOBODA

FCDD RLA TF
T EHLERS
L MAGNESS
C MEYER
D SCHEFFLER
FCDD RLA TG
N GNIAZDOWSKI
S KUKUCK
FCDD RLA S
A WEST
FCDD RLA V
F HUGHES
FCDD RLA VA
R EMERSON
FCDD RLA VB
A HALL
FCDD RLA W
T V SHEPPARD
FCDD RLA WE
T G BROWN
FCDD RLR A
D STEPP
FCDD RLR EW
R ANTHENIEN

4 (PDF) WHITING SCHOOL OF ENG
JOHNS HOPKINS UNIV
S BAILOOR
T D NGUYEN
B NOTGHI
KT RAMESH

5 (PDF) GEORGIA INST OF TECH
S KALIDINDI
S MARGULIES
D MCDOWELL
N THADHANI
M ZHOU

1 (PDF) DEPT OF ENGRNG SCI AND MECHANICS
VIRGINIA POLYTECHNIC INST AND STATE UNIV
R BATRA

4 (PDF) MASSACHUSETTS INST OF TECHLGY
INST FOR SOLDIER NANOTECHNOLOGIES
M J BUEHLER
R RADOVITZKY
C SCHUH
S SOCRATE

1 (PDF) DEPT OF MECHL AND NUCLEAR ENGRNG
THE PENNSYLVANIA STATE UNIV
R KRAFT

1 (PDF) INDIAN INST OF TECH
R BHARDWAJ

2 (PDF) CENTER FOR APPLIED BIOMECHANICS
UNIV OF VIRGINIA
M B PANZER
R SALZAR

1 (PDF) UCSD MAT SCI AND ENG
M MEYERS

1 (PDF) DUKE UNIV
BIOMED ENG
C R BASS

1 (PDF) UNIV OF CAPE TOWN
BLAST IMPACT & SURVIVABILITY UNIT
T J CLOETE

1 (PDF) UNIV OF OXFORD
BLAST IMPACT & SURVIVABILITY UNIT
C SIVIOUR

1 (PDF) UNIV OF CAMBRIDGE
ENG DEPT
V DESHPANDE
B LIU

4 (PDF) UNIV OF SOUTH CAROLINA
COL OF ENG
S RAJAN
S SOCKALINGAM
M SUTTON
F THOMAS

3 (PDF) DSM DYNEEMA PROTECTIVE MATERIALS
U HEISSERER
R ROZANSKY
H VAN DER WERFF

1 (PDF) IMPERIAL COL LONDON
DEPT OF PHYSICS
W PROUD

1 (PDF) DIV OF ENG AND APPL SCI
CALTECH
R RAVICHANDRAN

1 (PDF) DEPT OF AERO ENG AND ENG MECH
U TEXAS AUSTIN
K RAVI-CHANDAR

1 (PDF) AERO AND ASTRO ENG
PURDUE UNIV
W CHEN

1 (PDF) DEPT OF NEUROSURGERY
MED COL OF WISCONSIN
N YOGANANDAN

1 (PDF) SANDIA NATL LABS
B SANBORN

1 (PDF) WOLFSON SCHOOL OF MECHANICAL, ELECTRICAL, AND MANUFACTURING ENG
LOUGHBOROUGH UNIV
V SILBERSCHMIDT

1 (PDF) DEPT OF MECH AND AERO ENG
CASE WESTERN RESERVE UNIV
V PRAKASH

1 (PDF) MATERIALS SCI AND ENG
UNIV OF DELAWARE
J GILLESPI

1 (PDF) SIBLEY SCHOOL OF MECH AND AERO ENG
CORNELL UNIV
S L PHOENIX

1 (PDF) DUPONT
B VANARSDALEN

1 (PDF) DEPT OF MECH SCI AND ENG
UNIV OF ILLINOIS URBANA-CHAMPAIGN
I CHASIOTIS

1 (PDF) DEPT OF MECH ENG
UNIV OF CA SANTA BARBARA
S DALY

1 (PDF) CENTER FOR BIOENG AND BIOTECH
UNIV OF WATERLOO
D CRONIN

1 (PDF) DEPT OF MECH ENG
UNIV OF ALBERTA
J HOGAN

1 (PDF) LANGLEY RESEARCH CNTR
NASA
J CLINE

2 (PDF) LOS ALAMOS NATL LAB
E BROWN
G GRAY

1 (PDF) B SCOTT